Applied Thermal Engineering 50 (2013) 683–692

Contents lists available at SciVerse ScienceDirect

Applied Thermal Engineering

journal homepage: www.elsevier.com/locate/apthermeng

Thermodynamics and thermal stress analysis of thermoelectric power generator: Influence of pin geometry on device performance

A.S. Al-Merbati, B.S. Yilbas*, A.Z. Sahin

Mechanical Engineering Department, KFUPM, Box 1913, Dhahran 31261, Saudi Arabia

HIGHLIGHTS

- Thermal efficiency improves for certain range of pin geometry.
- Thermal stress in thermoelectric module varies for different configuration of pin geometry.
- Maximum stress occurs around the edges of the pins in the region close to the hot plate.
- The pin geometry with $R_A = 2$ results in slightly low thermal stress in the pin.

ARTICLE INFO

Article history:
Received 8 May 2012
Accepted 13 July 2012
Available online 25 July 2012

Keywords:
Thermoelectric
Power generation
Thermal stress
Efficiency

ABSTRACT

Thermodynamics and thermal stress analysis of thermo-electric power generator is carried out. The influence of device geometry on thermal stress, thermal efficiency and output power is examined. The finite element method is incorporated to predict temperature and stress fields in the thermo electric device. It is found that thermal efficiency improves for certain geometric configuration of the device. In this case; the maximum thermal stress developed in the pin reduces slightly indicating improved life expectation of the device.

© 2012 Elsevier Ltd. All rights reserved.

1. Introduction

Thermoelectric power generator is one of the solid-state devices converting thermal energy into an electrical energy. Thermoelectric generators operate in between the high and low temperature sources and the efficiency of the device increases with increasing temperature difference between the sources. However, thermal stress developed within the device limits temperature difference in the practical applications due to the shorting of the life cycle of the device. Moreover, material failure due to high stress induced cracking prevents further operations of the device with expected performance. Consequently, investigation into thermal stress development in the thermoelectric device becomes essential.

The efficiency of thermoelectric power generator under thermal cyclic loading was investigated by Hatzikraniotis et al. [1]. They indicated that cyclic thermal loading of the device resulted in reduction in Seebeck current and increased in electric and thermal resistivity. Thermal expansion of high temperature thermoelectric materials was investigated by the Ravi et al. [2]. They showed that thermal expansion coefficient of the thermoelectric materials was the critical parameter influencing stress levels in the device. A new method for thermoelectric power generation using large area p-n-junction was presented by Span et al. [3]. Their findings revealed that the new design of the device eliminated the thermal stress between active elements, such as pins, and joining material. Thermo-mechanical modeling of large area thermoelectric generators was carried out by Turenne et al. [4]. They indicated that the maximum stress was increased in the thermoelectric device close to the edge of the pins. Thermo-mechanical analysis of thermo-electric power generator was carried out by Soto and Venkatasubramanian [5]. They showed that due to the large temperature gradients as well as mismatch in thermal expansion coefficients, high stress levels were formed in the thermoelectric device. Thermal stress analysis for thermoelectric generator was carried out by Nakatani et al. [6]. The findings revealed aluminum and molybdenum coatings formed by atmospheric plasma spraying reduce the thermal stain at the interface of the pins. Thermal expansion in the thermoelectric generators was examined by Hilkage at [7]. They showed that the grain size in the active elements influenced significantly thermal expansion coefficient of

* Corresponding author. Tel.: +966 3 860 5223; fax: +966 3 860 2949.
E-mail address: bsyilbas@kfupm.edu.sa (B.S. Yilbas).

1359-4311/$ – see front matter © 2012 Elsevier Ltd. All rights reserved.
http://dx.doi.org/10.1016/j.applthermaleng.2012.07.021

the device pins. Thermal efficiency of the topping cycle with and without presence of thermoelectric generator was investigated by Sahin et al. [8]. They demonstrated that thermal efficiency of the topping cycle becomes slightly higher than that of the same system without the presence of the thermoelectric generators for a certain combination of operating and thermoelectric device parameters. Numerical modeling and design of thermoelectric cooling systems were carried out by Jou [9]. He introduced three approaches to obtain the internal parameters of a given thermoelectric module for designing of a thermoelectric cooling system. Thermoelectric cooling of microelectronic circuits and waste heat recovery were examined by Gould et al. [10]. They demonstrated that maximum electrical power could be generated by the thermoelectric module when a water cooled heat sink was used as the secondary heat sink, as this produced the greatest temperature difference between both sides of the module. The irreversible analysis of a multi-element thermoelectric generator system was carried out by Xiao et al. [11]. They indicated found that the existence of the irreversible heat convection process caused a large loss of heat exergy in the thermoelectric genetor system and using thermoelectric generators for low-grade waste heat recovery had a promising potential.

Although considerable research studies were carried out to examine the thermodynamic performance of the thermoelectric device, thermal stress developed due to temperature gradients is not given enough attention. In addition, the location of the maximum stress level in the thermoelectric device and stress the stres intesnity minimization through altering geometric configuration of device pins are left obscure in the previous studies. Consequently, in the present study, thermal efficiency and thermal stress developed in the thermoelectric generator are investigated. The temperature and stress fields in the device during the operation are stimulated using the finite element method. The influence of device pin geometry on the stress levels is examined and improvement in thermodynamic efficiency due to geometric configuration of the thermoelectric device is presented.

2. Mathematical analysis

The analysis pertinent to thermoelectric generator is divided into two-sub sections including the thermodynamic analysis and thermal stress formulations.

2.1. Thermodynamics analysis

The efficiency of the trapezoidal pin thermoelectric power generator, which is shown in Fig. 1 is given as [12]:

$$\eta = \frac{I^2 R_L}{\alpha I T_H + K(T_H - T_L) - \frac{1}{2} I^2 R} \tag{1}$$

where K is the thermal conductance and R is the electrical resistivity of the thermoelectric generator.

The current I is a function of Seebeck coefficient $\alpha = \alpha_p - \alpha_n$, the upper and lower junction (plate) temperatures (T_H and T_L), the electrical resistance R and the external load resistance R_L as

$$I = \frac{\alpha(T_H - T_L)}{R_L + R}, \tag{2}$$

Substituting equation (2) in equation (1) the efficiency becomes

$$\eta = \frac{\alpha^2 (T_H - T_L) R_L}{K(R_L + R)^2 + \alpha^2 T_H (R_L + R) - \frac{1}{2}\alpha^2 (T_H - T_L) R} \tag{3}$$

The cross-sectional area of the trapezoidal leg of the thermoelectric generator shown in Fig. 2 is

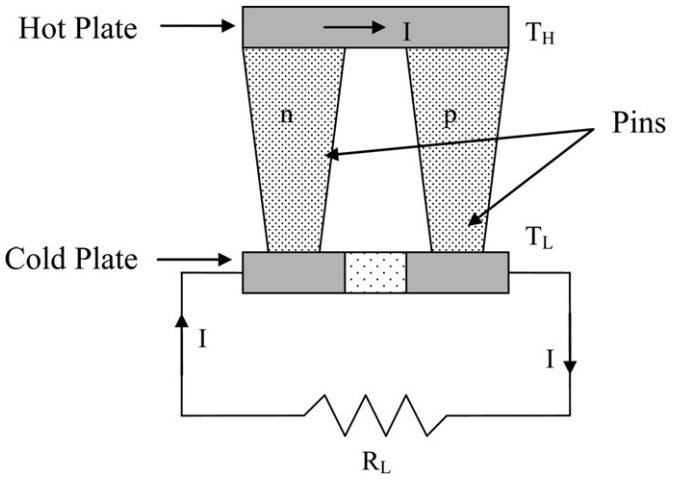

Fig. 1. Schematic view of a thermoelectric power generator and pin configurations.

$$A(x) = \frac{A_H - A_L}{L} x + A_L \tag{4}$$

where A_L is the cross sectional area of the bottom side of the leg and A_H is that of the top side. L is the height of the leg. Defining an area ratio $R_A = A_H/A_L$, the cross-sectional area of the leg can be written as

$$A(x) = A_0 \left[1 + 2 \frac{R_A - 1}{R_A + 1} \left(\frac{x}{L} - \frac{1}{2} \right) \right] \tag{5}$$

where A_0 is the cross-sectional area of the uniform leg.

The heat transfer rate through the leg along x is given by:

$$\dot{Q} = -kA(x) \frac{dT}{dx} \tag{6}$$

After assuming a steady heating situation and isolated leg surfaces, equation (6) can be re-arranged as

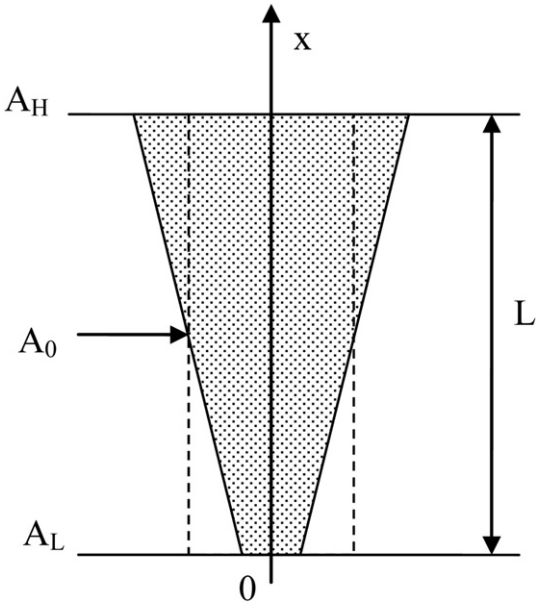

Fig. 2. Geometric configuration of the thermoelectric generator pin.

$$\dot{Q}\int_0^L \frac{dx}{A(x)} = -k\int_{T_L}^{T_H} dT \tag{7}$$

Making use of equation (5) in equation (7), and performing the integration

$$\dot{Q} = \frac{2k\frac{A_0}{L}\left(\frac{R_A-1}{R_A+1}\right)}{\ln(R_A)}(T_H - T_L) \tag{8}$$

Equation (8) indicates that the overall thermal conductance of the trapezoidal leg is

$$K_{leg} = \frac{2k\frac{A_0}{L}\left(\frac{R_A-1}{R_A+1}\right)}{\ln(R_A)} \tag{9}$$

Considering the two legs in Fig. 1, the total thermal conductance of the thermoelectric generator can be written as

$$K = 2(k_p + k_n)\frac{\frac{A_0}{L}\left(\frac{R_A-1}{R_A+1}\right)}{\ln(R_A)} \tag{10}$$

where k_p and k_n are the thermal conductivities of the p-type and n-type legs, respectively.

On the other hand, the overall electrical resistance of the leg can be written as

$$R_{leg} = \int_0^L \frac{dx}{kA(x)} \tag{11}$$

Substituting A(x) from equation (5) and performing the integration, the overall electrical resistance is obtained as

$$R_{leg} = \frac{1}{2k_e\frac{A_0}{L}\left(\frac{R_A-1}{R_A+1}\right)}\ln(R_A) \tag{12}$$

Similarly, considering the two legs the total electrical resistance of the thermoelectric generator becomes

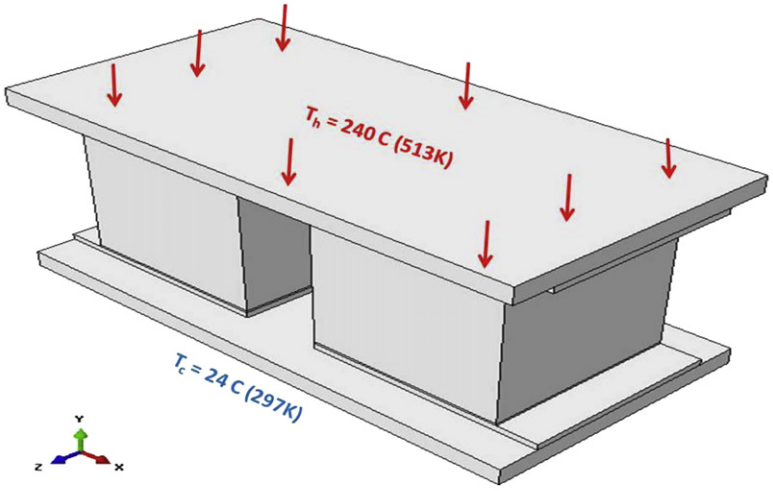

3-Dimensional view of thermoelectric generator

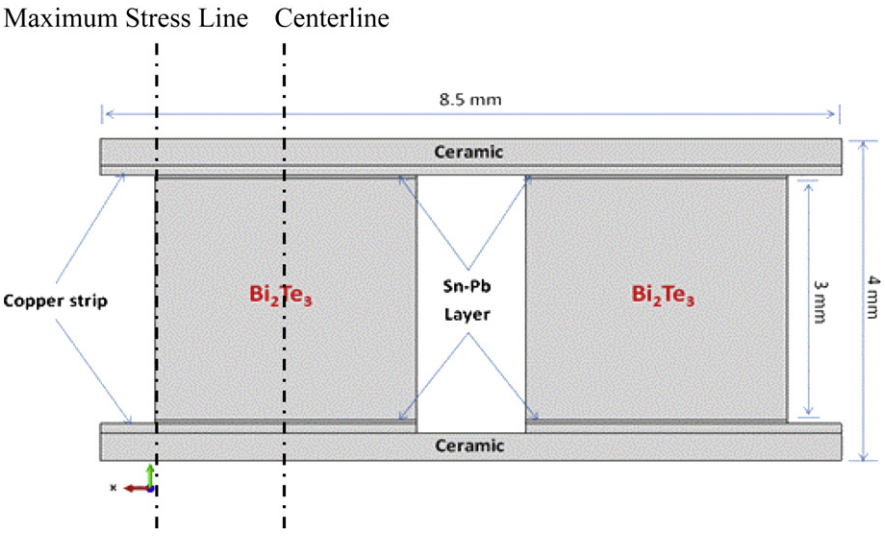

Fig. 3. Three-dimensional view of thermoelectric generator and its dimensions used in the simulations.

$$R = \left(\frac{1}{k_{e,p}} + \frac{1}{k_{e,n}}\right) \frac{1}{2\frac{A_0}{L}\left(\frac{R_A - 1}{R_A + 1}\right)} \ln(R_A) = \frac{k_{e,p} + k_{e,n}}{2k_{e,p}k_{e,n}\frac{A_0}{L}\left(\frac{R_A - 1}{R_A + 1}\right)} \ln(R_A) \quad (13)$$

where k_{ep} and k_{en} are the electrical conductivities of the p-type and n-type legs, respectively. Substituting equations (10) and (13) in equation (3) the efficiency of the thermoelectric generator can be written in dimensionless form as

$$\eta = (1+\theta)\frac{2ZT_{ave}\left(1+\sqrt{\frac{r_k}{r_{ke}}}\right)^2\left(\frac{R_L}{R_0}\right)}{(1+\theta)\left(\frac{K}{K_0}\right)\left(\frac{R_L}{R_0}+\frac{R}{R_0}\right)^2 + 2ZT_{ave}\left(1+\sqrt{\frac{r_k}{r_{ke}}}\right)^2\left[\frac{R_L}{R_0}+\frac{1}{2}\frac{R}{R_0}(1+\theta)\right]} \quad (14)$$

where

$$\theta = \frac{T_L}{T_H}, \text{(Temperature ratio)} \quad (15)$$

$$r_k = \frac{k_p}{k_n}, \text{(Thermal conductivity ratio)} \quad (16)$$

$$r_{ke} = \frac{k_{e,p}}{k_{e,n}}, \text{(Electrical conductivity ratio)} \quad (17)$$

$$ZT_{ave} = \frac{\alpha^2\left(\frac{k_{e,n}}{k_n}\right)T_H}{\left(1+\sqrt{\frac{r_k}{r_{ke}}}\right)^2}\left(\frac{1+\theta}{2}\right)$$

(The figure of merit based on the average temperature) (18)

$$K_0 = \frac{A_0 k_n}{L} \text{(Reference thermal conductance)} \quad (19)$$

and

$$R_0 = \frac{L}{A_0 k_{e,n}} \text{(Reference electrical resistivity)}. \quad (20)$$

Thus, the overall thermal conductance and overall electrical resistivity can be written in dimensionless form, respectively, as

$$\frac{K}{K_0} = 2\frac{(r_k+1)}{\ln(R_A)}\left[\frac{R_A-1}{R_A+1}\right] \quad (21)$$

and

$$\frac{R}{R_0} = \left(\frac{1+r_{ke}}{r_{ke}}\right)\frac{\ln(R_A)}{2\left[\frac{R_A-1}{R_A+1}\right]} \quad (22)$$

Table 1
Properties of Bi_3Te_2 used for the efficiency calculation.

R_L/R_0	10
ZT_{ave}	0.9
r_k	1.25
$r_{k,e}$	1.2
θ	300/550

Table 2
Properties of Bi_2Te_3 [15–17].

Temperature (K)		Thermal conductivity (W/m-K)
325		0.93
375		0.9
425		0.91
475		0.95
525		1.1
Specific heat (J/K-kg)	**Density (kg/m-3)**	**Yield stress (Pa)**
154.4	7740	1.12E+08
Thermal expansion (/K)		**Temperature (K)**
8.00E-06		297
1.01E-05		304.3
1.21E-05		365
1.24E-05		451
1.32E-05		613
1.33E-05		793
1.41E-05		864
Poisson's ratio	**Young's modulus (Pa)**	**Temperature (K)**
0.23	6.5E + 010	200
0.23	6.3E + 010	300
0.23	6.2E + 010	400
0.23	6.0E + 010	500
0.23	5.9E + 010	600

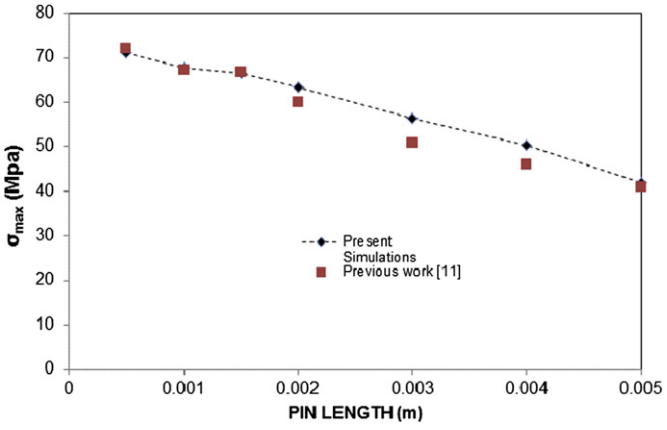

Fig. 4. Validation of present simulations with the previous study [11].

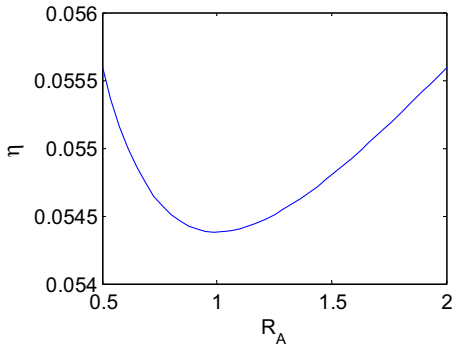

Fig. 5. Thermal efficiency variation with RA (pin area ratio of at hot junction to cold junction, $R_A = A_H/A_L$.

2.2. Thermal stress formulations

Fig. 3 shows the schematic view of three-dimensional thermoelectric generator. The thermoelectric module has inhomogeneous thermal and mechanical properties in the z-direction since the properties used in this study are temperature dependent. The transient heat conduction equation considered is:

$$\frac{\partial}{\partial x}\left[k(z)\frac{\partial T}{\partial x}\right] + \frac{\partial}{\partial y}\left[k(z)\frac{\partial T}{\partial y}\right] + \frac{\partial}{\partial z}\left[k(z)\frac{\partial T}{\partial z}\right] = c_p\rho\frac{\partial T}{\partial t} \tag{23}$$

The coupled thermal stress analysis require to identify the displacement–strain relations, which are expressed in dimensionless form as follows [13]:

$$\bar{\varepsilon}_{xx} = \frac{\partial \bar{u}}{\partial \bar{x}}, \quad \bar{\varepsilon}_{yy} = \frac{\partial \bar{v}}{\partial \bar{y}}, \quad \bar{\varepsilon}_{zz} = \frac{\partial \bar{w}}{\partial \bar{z}} \tag{24}$$

$$\begin{aligned} \bar{\varepsilon}_{xy} &= \frac{1}{2}\left(\frac{\partial \bar{u}}{\partial \bar{y}} + \frac{\partial \bar{v}}{\partial \bar{x}}\right), \quad \bar{\varepsilon}_{yz} = \frac{1}{2}\left(\frac{\partial \bar{v}}{\partial \bar{z}} + \frac{\partial \bar{w}}{\partial \bar{y}}\right), \\ \bar{\varepsilon}_{zx} &= \frac{1}{2}\left(\frac{\partial \bar{u}}{\partial \bar{z}} + \frac{\partial \bar{w}}{\partial \bar{x}}\right) \end{aligned} \tag{25}$$

An exact implementation of Newton's method involves a nonsymmetrical Jacobian matrix which is stress–strain relation in dimensionless form as is illustrated in the following matrix representation of the coupled equations [13]:

$$\begin{Bmatrix} \bar{\sigma}_{xx} \\ \bar{\sigma}_{yy} \\ \bar{\sigma}_{zz} \\ \bar{\sigma}_{yz} \\ \bar{\sigma}_{zx} \\ \bar{\sigma}_{xy} \end{Bmatrix} = \frac{\bar{E}}{(1+\nu)(1-2\nu)} \begin{bmatrix} 1-\nu & \nu & \nu & 0 & 0 & 0 \\ \nu & 1-\nu & \nu & 0 & 0 & 0 \\ \nu & \nu & 1-\nu & 0 & 0 & 0 \\ 0 & 0 & 0 & 1-2\nu & 0 & 0 \\ 0 & 0 & 0 & 0 & 1-2\nu & 0 \\ 0 & 0 & 0 & 0 & 0 & 1-2\nu \end{bmatrix} \begin{Bmatrix} \bar{\varepsilon}_{xx} \\ \bar{\varepsilon}_{yy} \\ \bar{\varepsilon}_{zz} \\ \bar{\varepsilon}_{yz} \\ \bar{\varepsilon}_{zx} \\ \bar{\varepsilon}_{xy} \end{Bmatrix} - \begin{Bmatrix} 1 \\ 1 \\ 1 \\ 0 \\ 0 \\ 0 \end{Bmatrix} \frac{\bar{\alpha}\bar{E}\bar{T}}{1-2\nu} \tag{26}$$

Solving this system of equations requires the use of the unsymmetrical matrix storage and solution scheme. Furthermore, the mechanical and thermal equations are solved simultaneously.

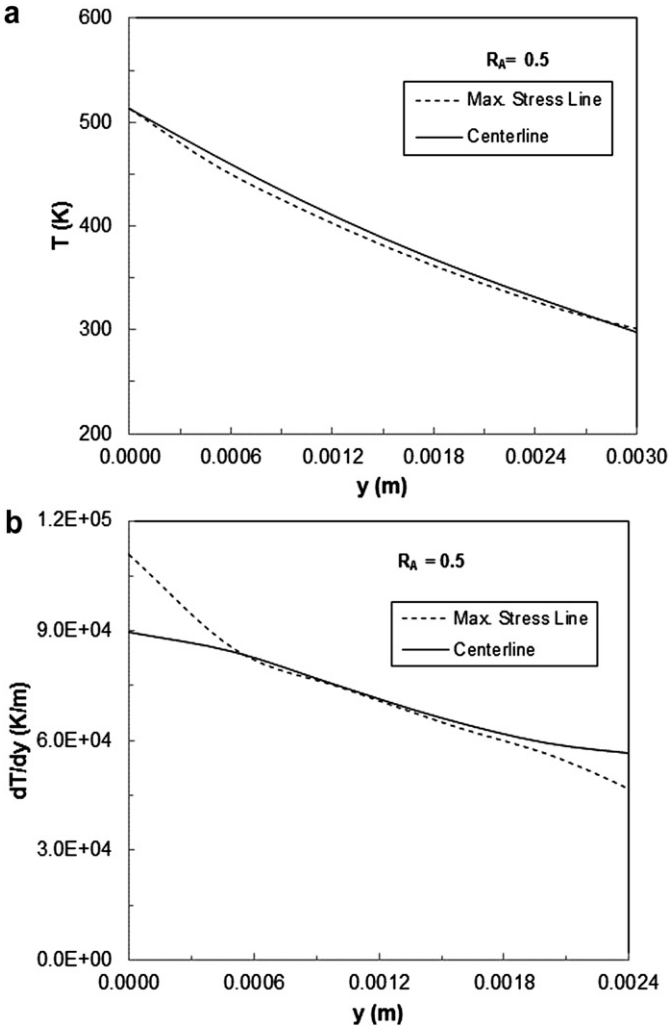

Fig. 6. (a)Temperature distribution along the centerline and the maximum stress line for $R_A = 0.5$.(b)Temperature gradient along the centerline and the maximum stress line for $R_A = 0.5$.

3. Numerical simulations

The thermal efficiency, which is presented in equation (14) is simulated using the data in Table 1. For the thermal stress analysis ABAQUS finite element code [14] is used to simulate temperature and stress fields in the thermoelectric generator. Table 2 gives the data used in the simulations.

In the thermal stress analysis simulations, it is considered that the thermoelectric generator consists of ceramic substrate, copper plate, tin-Lead solder, and thermoelectric pins (Fig. 3). It is also considered that the thickness of copper plate is 0.12 mm, the thickness of solder is 0.04 mm, and the thickness of ceramic substrate is 0.34 mm. The size of the thermoelectric generator pins is 3 mm × 3 mm × 3 mm (Fig. 3). In the thermal stress simulations, it is assumed that the thermoelectric pins are made from Bi_2Te_3 and that there is no difference in properties as a function of position, so that the thermoelectric and mechanical properties are function of temperature only. The thermal conductivity k (T), coefficient of liner thermal expansion α (T), specific heat capacity c_p (T), and modulus of elasticity E (T) are the function of temperature.

To validate the predictions of thermal stress analysis, simulations are extended to include the case, which was presented in the early study [15]. In this case, simulations conditions are re-set to be in line with the previous study [15] the data used in the previous study are incorporated in the simulations. The thermal stress predictions of the present study and the results of the previous study is shown in Fig. 4. It is evident that both results are in good agreement. Therefore, the model used in the present study is justifiable to proceed with the predictions of thermal stress fields in the thermoelectric generator.

4. Results and discussion

Thermodynamic analysis and thermal stress field developed in the thermoelectric generator are investigated and the influence of pin geometric configuration on thermal efficiency and thermal stress levels are examined.

Fig. 5 shows efficiency variation with the geometric parameter R_A, which is the area ratio of the pin cross-section at cold junction

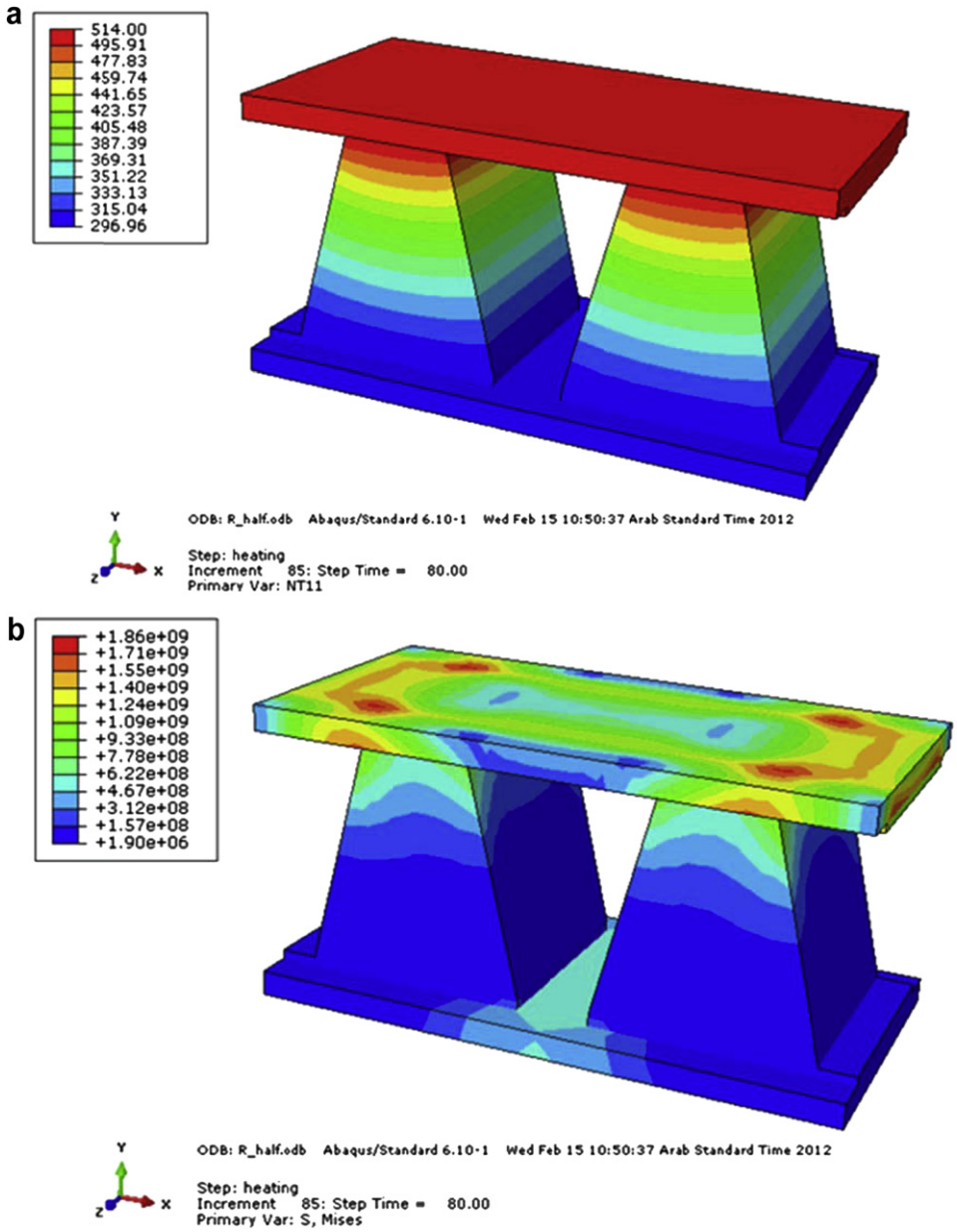

Fig. 7. (a)Three-dimensional temperature distribution in the thermoelectric generator for $R_A = 0.5$.(b)Three-dimensional thermal stress distribution in the thermoelectric generator for $R_A = 0.5$.

to hot junction ($R_A = A_H/A_L$). It can be observed that thermal efficiency of the thermoelectric generator increases for R_A values different than $R_A = 1$ and the minimum efficiency occurs for $R_A = 1$. This indicates that parallel sided pins for the thermoelectric generator are not always the optimum design for the maximum efficiency. Consequently, the pin design including either $R_A \leq 0.5$ and $R_A \leq 2$ results in improved thermal efficiency. Although the improvement in thermal efficiency is low, small improvement of thermal efficiency for one device adds to the improvement of the overall thermal efficiency of all devices in series, which are used for the practical applications.

Fig. 6(a) shows temperature distribution along the two lines in the y-axis for $R_A = 0.5$. The centerline represents the line passing through the pin center along the y-axis (Fig. 3) and maximum stress line corresponds to the line passing through the maximum stress locations along the y-axis (Fig. 3). Temperature distribution is presented when the temperature in the pin reaches to a steady state distribution. It should be noted that the transient heating takes place only 0.3 s after the heating is initiated and temperature field settles through heat in the thermoelectric device including the pins. The temperature decays gradually along the pin height for both lines in the y-axis. However, the temperature gradients differ totally along these lines, which are evident from Fig. 6(b), in which the temperature gradient along the y-axis is shown. The temperature gradient attains high values in the region close to the hot junction of the pin, which is more pronounced along the maximum stress line. However, the temperature gradient reduces toward the cold junction of the pin. When comparing the temperature gradients along both lines; it is evident that the temperature gradient is higher in hot junction of the pin along the maximum stress line as compared to that of the center line. However, opposite is true in the region toward the cold junction. Consequently, large changes in the temperature gradient results development of high strain in the pin. Fig. 7(a) shows temperature contours in the thermoelectric generator and the pins. It is evident that temperature remains almost uniform along the *x* and *z*-axes. The large variation in the temperature occurs along the y-axis between the hot and cold junctions.

Fig. 8 shows thermal stress variation along the centerline and the maximum stress line in the y-direction for $R_A = 0.5$. It is evident that thermal stress attains high values in the region of the hot junction which is particularly true along the maximum stress line. Thermal stress reduces sharply in the region close to the hot junction in the pin and its decay become gradual toward the cold junction. The sharp decay of thermal stress is attributed to attainment of high temperature gradients in this region. Fig. 7(b) shows thermal stress contours in the thermoelectric device and its pins. High stress region occurs locally in the pin, particularly at the edges of the pin where pin is attached to high temperature plate. The attainment of high stress is because of one on all of the following reasons: i) high temperature gradient developed in this region gives to high thermal stress levels, and ii) the difference in thermal expansion coefficients due to pin and the hot plate which generates high stress levels at the interface location between the hot plate and the pin. Moreover, low stress region in the pin extends toward the cold junction region.

Fig. 9(a) shows temperature distribution along the centerline and the maximum stress line along the y-axis for $R_A = 1$. It should be noted that $R_A = 1$ corresponds to rectangular parallel pin geometry. Temperature variation between the hot and the cold junctions along the both lines is gradual, provided that the temperature gradient changes significantly in the hot plate region for both lines (Fig. 9b). In this case the temperature gradient attains higher values in the vicinity of the hot plate, where $y \cong 0$, for the maximum stress line as compared to that corresponding to the centerline. The high temperature gradient generates high strain in this region. Fig. 10(a) shows temperature contours in the thermoelectric generator and the pins. It is evident that temperature variation along *x* and *z*-axes are almost uniform. However, temperature variation along the y-axis is large due to the presence of hot and cold plates across the pins.

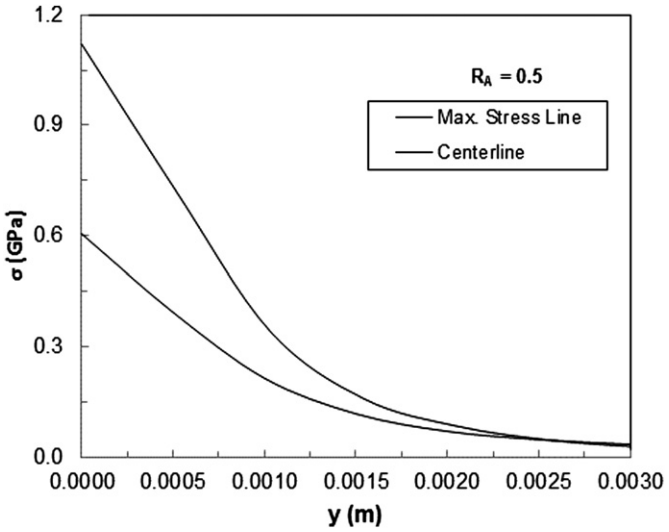

Fig. 8. Thermal stress distribution along the centerline and the maximum stress line for $R_A = 0.5$.

Fig. 11 shows thermal stress distribution along the centerline and the maximum stress line in the y-axis for $R_A = 1$. Thermal stress

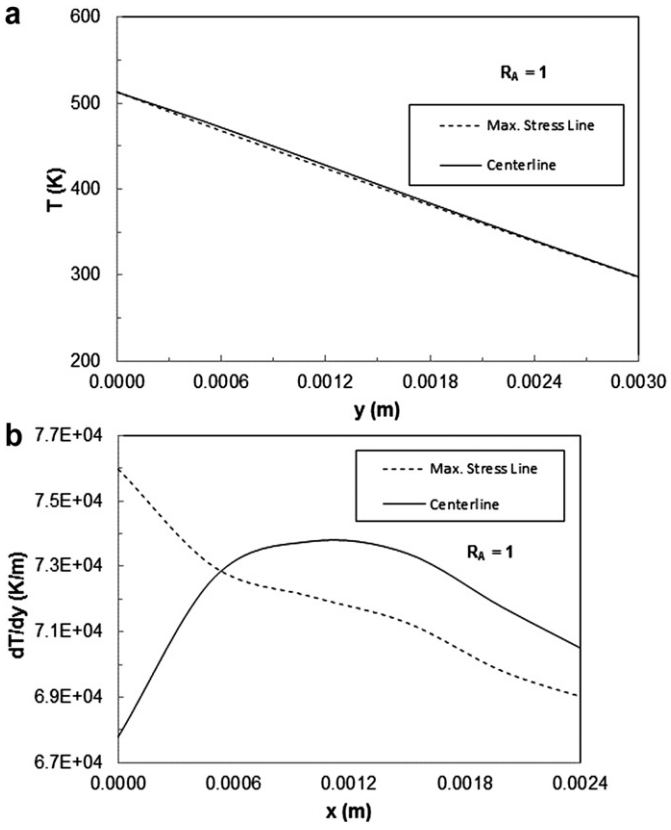

Fig. 9. (a)Temperature distribution along the centerline and the maximum stress line for $R_A = 1$.(b)Temperature gradient distribution along the centerline and the maximum stress line for $R_A = 1$.

varies significantly along the both lines and stress reduces slightly in the region next to the hot plate and increases gradually with increasing distance toward the cold plate. However, thermal stress reduces sharply in the region close to the hot plate along the maximum stress line and the decay becomes gradual toward the cold plate. The attainment of high stress along maximum stress line is due to thermal expansion of the pin and high temperature gradient developed in the region close to the hot plate. Fig. 10(b) shows thermal stress counters in the thermoelectric generator and its pins. It can be observed that high stress region is locally developed toward the pin edges, particularly in the region next to the hot plate. However, thermal stress drops significantly toward to the cold plate due to attainment of the low temperature gradients in this region.

Fig. 12(a) shows temperature distribution along the centerline and the maximum stress line in the y-axis for $R_A = 2$. Temperature decays gradually along the both lines form the high temperature plate to low temperature plate as similar those shown in Figs. 6 and 9(a). However, temperature along the maximum stress line attains slightly higher values than that of the centerline. This is associated with the heat conduction along the thermoelectric pins. Moreover, the temperature gradient increases gradually toward the cold plate, which is associated with the gradual decay of temperature along the both lines (Fig. 12(b)). The temperature gradient along the maximum stress line is slightly lower than that of along the centerline. This indicates the attainment of relatively lower thermal strain along this line. Fig. 13(a) shows temperature contours in the thermoelectric device and in the pins. Temperature variation is almost uniform along the x and z-axes as similar to those obtained for the cases $R_A = 0.5$ and $R_A = 1$.

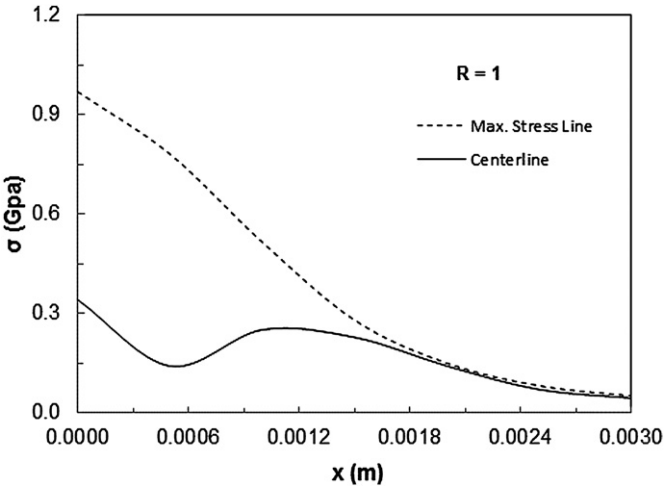

Fig. 11. Thermal stress distribution along the centerline and the maximum stress line for $R_A = 1$.

Fig. 14 shows von Mises Stress distribution along the centerline and the maximum stress line in the y-axis direction for $R_A = 2$. Thermal stress behavior is similar to that shown in Fig. 11 for $R_A = 1$, provided that the maximum stress at $x = 0$ is less than that of $R_A = 1$. This is attributed to the differences in the temperature gradient behavior particularly in the region close to the hot plate.

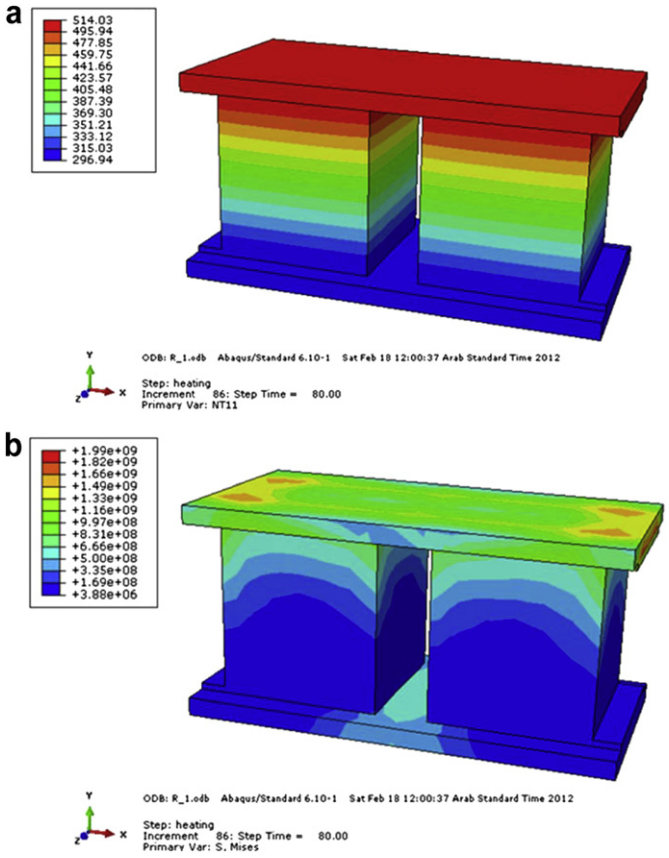

Fig. 10. (a)Three-dimensional temperature distribution in the thermoelectric generator for $R_A = 1$.(b)Three-dimensional thermal stress distribution in the thermoelectric generator for $R_A = 1$.

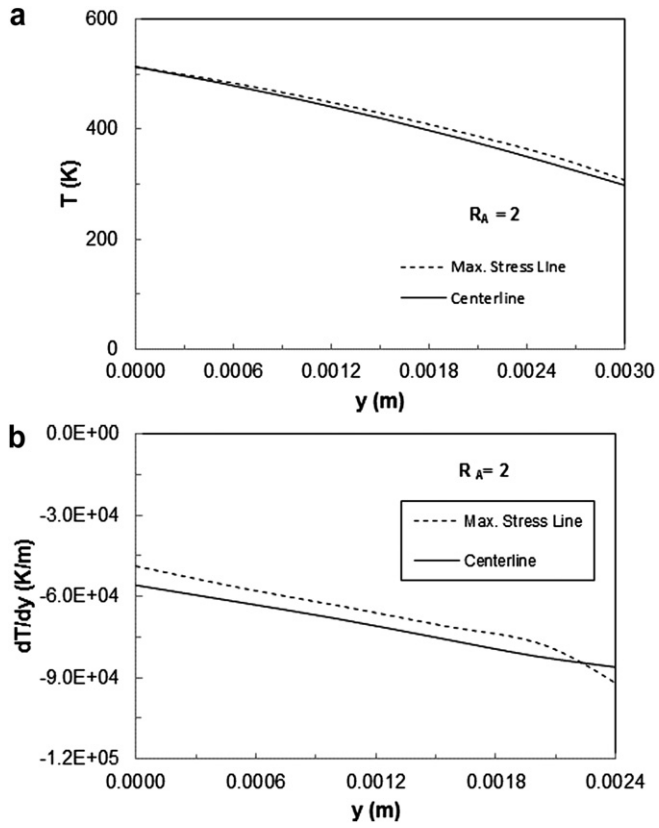

Fig. 12. (a)Temperature distribution along the centerline and the maximum stress line for $R_A = 2$.(b)Temperature gradient distribution along the centerline and the maximum stress line for $R_A = 2$.

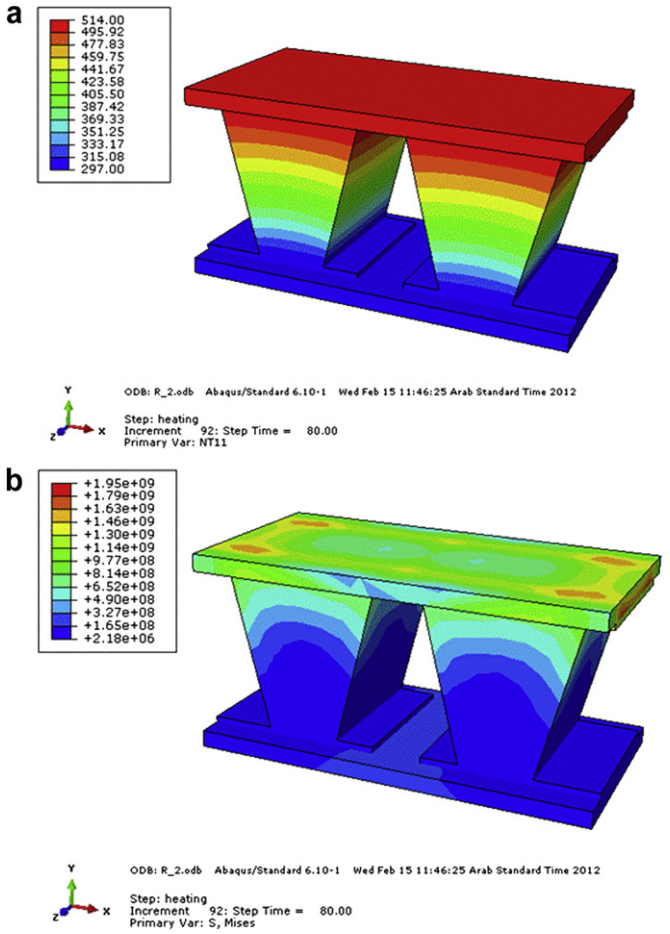

Fig. 13. (a)Three-dimensional temperature distribution in the thermoelectric generator for $R_A = 2$.(b)Three-dimensional thermal stress distribution in the thermoelectric generator for $R_A = 2$.

Fig. 13(b) shows thermal stress contours in the thermoelectric generator and in the pins. Thermal stress is high in the region close to the hot plate and reduces sharply in the region close to the cold plate. The presence of high stress centers in the region of the pin edges is evident. This is attributed to the attainment of high temperature gradient and thermal expansion coefficient differences between the hot plate and the pin material. Table 3 gives the

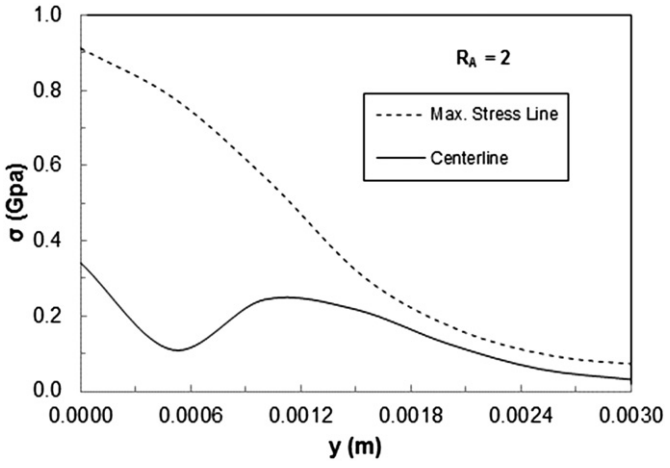

Fig. 14. Thermal stress distribution along the centerline and the maximum stress line for $R_A = 2$.

Table 3
Comparison of the maximum and the minimum stresses predicted from the present study and obtained from the previous study [15].

	$R_A = 0.5$	$R_A = 1$	$R_A = 2$
Max. stress (GPa)	1.12	0.969	0.912

maximum values of thermal stress developed in the thermoelectric generator when the device operation reaches to steady state condition. The maximum thermal stress for $R_A = 2$ is the minimum among the other cases. This suggests that changing the design of the pins of the thermoelectric power generators form parallel to trapezoidal geometry, the maximum thermal stress developed can be reduced. Although the reduction is small, the life extension of the thermoelectric device is possible.

5. Conclusion

Thermodynamic and thermal stress analysis of thermoelectric generator is carried out for various device pin centrifugations. In the analysis, the properties of Bi_2Te_3 thermoelectric material are used. It is found that thermal efficiency of the thermoelectric generator improves for $R_A \leq 0.5$ and $R_A \leq 2$. Although this improvement is small, its effect becomes high for the series operation of many thermoelectric devices. Temperature variation in the x,y plane does not alter significantly; in which case, almost uniform temperature distribution takes place along the pins. Temperature variation along the y-axis results in sharp decay of temperature in the region close to the hot plate. This gives rise to attainment of high temperature gradients in this region. Thermal stress developed in the thermoelectric module and its pins varies for different configuration of pin geometry and the maximum stress occurs around the edges of the pins, which is more produced in the region close to the hot plate. The attainment of high stress levels in this region is attributed to the high temperature gradients and the mismatch of thermal expansion coefficients of the hot plate and the device pins. The influence of pin geometry on temperature gradients and thermal stress is notable. In this case the pin with $R_A = 2$ results in slightly low thermal stress in the pin. This indicates that changing the pin geometry improves temperature variation in the thermoelectric generator while suppressing the maximum stress levels in the pin. Consequently, life expectation of the device can be improved with geometric design of the device pins. In addition, for pin geometric configuration $R_A = 2$, thermal efficiency of the device also improves.

Acknowledgements

The authors acknowledge the funded project# RG 1204 via support of Thermoelectric Group formed by the Deanship of Scientific Research and Center of Excellence for Scientific Research Collaboration with MIT and King Fahd University of Petroleum and Minerals, Dhahran, Saudi Arabia for this work.

References

[1] E. Hatzikraniotis, K.T. Zorbas, I. Samaras, T. Kyratsi, K.M. Paraskevopoulos, Efficiency study of a commercial thermoelectric power generator (TEG) under thermal cycling, J. Electron. Mater. 39 (2010) 2112–2116.
[2] V. Ravi, S. Firdosy, T. Caillat, E. Brandon, K. Van Der Walde, L. Maricic, A. Sayir, Thermal expansion studies of selected high-temperature thermoelectric materials, J. Electron. Mater. 38 (2009) 1433–1442.
[3] G. Span, M. Wagner, S. Holzer, T. Grasser, Thermoelectric power conversion using generation of electron-hole pairs in large area p-n junctions, ICT'06-25th International Conference on Thermoelectrics, August 6-August 10, 2006, Proceedings, (2006) 23–28.
[4] S. Turenne, T. Clin, D. Vasilevskiy, R.A. Masut, Finite element thermo-mechanical modeling of large area thermoelectric generators based on bismuth telluride alloys, J. Electron. Mater. 39 (2010) 1926–1933.

[5] M.A. Soto and R. Venkatasubramanian, ANSYS-based detailed thermo-mechanical modeling of complex thermoelectric power designs, Int. Conference on Thermoelectrics, ICT, Proceedings, (2005) 204–206.
[6] Y. Nakatani, R. Takaku, T. Hino, T. Shindo, Y. Itoh, Mechanical aspects of structural optimization in a Bi-Te thermoelectric module for power generation, Mater. Res. Soc. Symp. Proc. 842 (2005) 413–418.
[7] Y. Hikage, S. Masutani, T. Sato, S. Yoneda, Y. Ohno, Y. Isoda, Y. Imai, Y. Shinohara, Thermal expansion properties of thermoelectric generating device component, Int. Conference on Thermoelectrics, ICT'07, Proceedings (2007). 331–335.
[8] A.Z. Sahin, B.S. Yilbas, S.Z. Shuja, O. Momin, Investigation into topping cycle: thermal efficiency with and without presence of thermoelectric generator, Energy 36 (2011) 4048–4054.
[9] R. Jou, Numerical modeling and design of thermoelectric cooling systems, Appl. Mechanics Mater. 110-116 (2012) 2639–2646.
[10] C.A. Gould, N.Y.A. Shammas, S. Grainger, Taylor thermoelectric cooling of microelectronic circuits and waste heat electrical power generation in a desktop personal computer, Mater. Sci. Eng. B 176 (2011) 316–325.
[11] H. Xiao, X. Gou, S. Yang, Detailed modeling and rrreversible transfer process analysis of a multi-element thermoelectric generator system, J. Electron. Mater. 40 (2011) 1195–1201.
[12] B.S. Yilbas, A.Z. Sahin, Thermoelectric device and optimum external load parameter and slenderness ratio, Energy 35 (2010) 5380–5384.
[13] Y. Ootao, Y. Tanigawa, Three-dimensional solution for transient thermal stresses of functionally graded rectangular plate due to nonuniform heat supply, Int. J. Mech. Sci. 47 (2005) 1769–1788.
[14] ABAQUS, Theory Manual, Version 6.9, ABAQUS Inc., Pawtucket, USA, 2009.
[15] J. Gao, Q. Du, X. Zhang, X. Jiang, Thermal stress analysis and structure parameter selection for a Bi2Te3-based thermoelectric module, J. Electron. Mater. 40 (2011) 884–888.
[16] L. Zhao, B. Zhang, J. Li, M. Zhou, W. Liu, J. Liu, Thermoelectric and mechanical properties of nano-SiC-dispersed Bi2Te3 fabricated by mechanical alloying and spark plasma sintering, J. Alloys and Compounds 455 (2008) 259–264.
[17] Y. Tong, F. Yi, L. Liu, P. Zhai, Q. Zhang, Molecular dynamics study of mechanical properties of bismuth telluride nanofilm, Physica B-Condens. Matter 405 (2010) 3190–3194.